Infection, Genetics and Evolution 73 (2019) 401–410

Contents lists available at ScienceDirect

Infection, Genetics and Evolution

journal homepage: www.elsevier.com/locate/meegid

Research paper

Comparative analysis of putative novel microRNA expression profiles induced by enterovirus 71 and coxsackievirus A16 infections in human umbilical vein endothelial cells using high-throughput sequencing

Jie Song[1], Yajie Hu[1], Huiwen Zheng, Lei Guo, Xing Huang, Xi Jiang, Weiyu Li, Jiaqi Li, Zening Yang, Shaozhong Dong*, Longding Liu*,[2]

Yunnan Key Laboratory of Vaccine Research & Development on Severe Infections Disease, Institute of Medical Biology, Chinese Academy of Medical Science and Peking Union Medical College, Kunming 650118, China

ARTICLE INFO

Keywords:
Hand, foot and mouth disease (HFMD)
Enterovirus 71 (EV71)
Coxsackievirus A16 (CA16)
microRNAs (miRNAs)
High-throughput sequencing

ABSTRACT

Hand, foot and mouth disease (HFMD) is mainly caused by human enterovirus 71 (EV71) and coxsackievirus A16 (CA16), which circulate alternatively or together in epidemic areas. Although the two viruses exhibit genetic homology, their clinical manifestations have some discrepancies. However, the factors underlying these differences remain unclear. Herein, we mainly focused on the alterations and roles of putative novel miRNAs in human umbilical vein endothelial cells (HUVECs) following EV71 and CA16 infections using high-throughput sequencing. The results identified 247 putative novel, differentially expressed miRNAs, of which only 11 miRNAs presented an opposite trend between the EV71- and CA16-infected samples and were used for target prediction. Gene ontology (GO) and pathway enrichment analysis of the predicted targets displayed the top 15 significant biological processes, molecular functions, cell components and pathways. Subsequently, regulatory miRNA-predicted targets and miRNA-GO and miRNA-pathway networks were constructed to further reveal the complex regulatory mechanisms of the miRNAs during infection. Therefore, our data provide useful insights that will help elucidate the different host-pathogen interactions following EV71 and CA16 infections and may offer novel therapeutic targets for these infections.

1. Introduction

Human enterovirus type 71 (EV71) and coxsackievirus A group type 16 (CA16) belong to human Enterovirus Species A of the *Enterovirus* genus within family *Picornaviridae*. These viruses are recognized as the predominant causative agents of hand, foot, and mouth disease (HFMD) in infants and young children, especially those < 5 years of age (Mao et al., 2014; Solomon et al., 2010). Although the symptoms of most HFMD cases are mild, including fever, loss of appetite, and a rash with blisters, and do not need specific treatment, a small percentage of cases progress to severe neurological diseases, such as fatal encephalitis, aseptic meningitis and acute flaccid paralysis, which may occasionally cause permanent paralysis or death (Ong and Wong, 2015). The occurrence of rare and life-threatening cases has propelled this common condition into the spotlight as a serious public health problem in affected countries (Reed and Cardosa, 2016). Vaccination is probably the most efficient approach for controlling HFMD epidemics (Pourianfar and Grollo, 2015). Currently, EV71 vaccines from three manufacturers [The Institute of Medical Biology, Chinese Academy of Medical Science (CAMS), Sinovac Biotech Ltd. (Sinovac) and Beijing Vigoo Biological Co., Ltd. (Vigoo)] have been approved by the China Food and Drug Administration (CFDA) (Mao et al., 2016). These vaccines showed high efficacy and satisfactory safety in providing protection against EV71-associated disease, but they could not effectively control the HFMD epidemic caused by other enterovirus infections, including CA16 (Wang et al., 2014). Over the past few decades, EV71 and CA16 have mostly been found cocirculating in the Asian-Pacific region (He et al., 2017). Thus, investigating differences between EV71 and CA16 infections and developing a broad-spectrum vaccine against HFMD are highly desirable goals to control the overall HFMD epidemic.

Currently, several studies have demonstrated that ectopic microRNA (miRNA) expression induced by EV71 infection can directly

* Corresponding authors.
E-mail addresses: dsz@imbcams.com.cn (S. Dong), longdingl@gmail.com (L. Liu).
[1] These authors contributed equally to this work.
[2] Lead contact.

https://doi.org/10.1016/j.meegid.2019.06.007
Received 13 February 2019; Received in revised form 3 June 2019; Accepted 4 June 2019
Available online 05 June 2019

target the viral genome or host genes, leading to cellular or tissue malfunctions and viral pathogenesis. For instance, host miR-296-5p and miR-23b both inhibit EV71 replication by targeting the viral genome to reduce EV71 infection (Wen et al., 2013; Zheng et al., 2013). EV71 has also been shown to induce the expression of miR-141, which can target the eIF4E translation initiation factor to downregulate host protein synthesis (Ho et al., 2011). Furthermore, our previous studies revealed significant differential miRNA expression changes in EV71- and CA16-infected human cells, such as human bronchial epithelial (16HBE) cells, rhesus monkey peripheral blood mononuclear cells (PBMCs) and human umbilical vein endothelial cells (HUVECs) (Hu et al., 2016; Hu et al., 2017; Song et al., 2017). In the present study, we further evaluate putative novel differentially expressed miRNAs in HUVECs infected with EV71 and CA16 using high-throughput sequencing technology and investigate the underlying mechanisms of these phenomena following EV71 and CA16 infections.

2. Materials and methods

2.1. Viral infections and cell line culture

HUVECs purchased from Jennino Biological Technology (Guangzhou, China) were cultivated in Dulbecco's modified Eagle's medium (DMEM) (Gibco, USA) supplemented with 10% fetal bovine serum (FBS, Gibco, USA) plus penicillin and streptomycin and incubated overnight at 37 °C in a humidified incubator with 5% CO_2. After the cells attached to the culture flask wall, the culture medium was renewed every 1–2 days. When the cells were 90% confluent, 0.25% trypsin (Sigma, USA) was used for digestion and subculture.

For the in vitro virus infections, the EV71 virus strain (subgenotype C4, GenBank: EU812515.1), which originated from an epidemic in Fuyang, China, in 2008, and the CA16 virus G20 strain (subgenotype B, GenBank: JN590244.1), which originated from an HFMD patient in Guangxi in 2010, were propagated in HUVECs at a multiplicity of infection (MOI) of 1 after 1 day of culture. The cells were infected in triplicate and collected at 0, 72 and 96 h post-infection (hpi). Cells infected with EV71 and CA16 for 0 hpi were used as the controls. We defined the different experimental groups as EV71–0 h, EV71–72 h, EV71–96 h, CA16–0 h, CA16–72 h and CA16–96 h. Additionally, a subset of the EV71–0 h and CA16–0 h groups was subjected to normalization (the normalization value was set to 1); these two groups were designated Con.

2.2. RNA isolation and quality control

miRNAs were extracted from the above samples using the mirVana™ miRNA Isolation Kit (Invitrogen, CA, USA) according to the manufacturer's instructions. The RNA integrity was checked using RNA 6000 Nano LabChips on an Agilent 2100 Bioanalyzer (Agilent Technologies, USA). The RNA quality was further checked by 1% agarose gel electrophoresis. Only samples with preserved 18S and 28S peaks and RNA integrity number (RIN) values > 7 were selected for the miRNA profile analysis. Qualified miRNAs from three independent experiments per group were mixed together and used for subsequent library construction and deep sequencing.

2.3. Small RNA library preparation, high-throughput sequencing and miRNA-seq data analysis

Small RNA library construction and sequencing were carried out by the National Engineering Center for Biochips in Shanghai on the Illumina Hi-Seq 2000 platform system (Illumina Inc., USA). For all samples, small RNA libraries were constructed using the TruSeq Small RNA sample preparation kit (Illumina, USA) following the manufacturer's protocol with 2 μg of RNA input per sample, followed by RNA 3′ adapter ligation, RNA 5′ adapter ligation, cDNA synthesis, PCR amplification using unique barcode sequences for each sample and gel-size selection of the small RNA library. Then, six small RNA libraries were used for deep sequencing with the Illumina HiSeq™ technology. Raw sequences were processed by filtering out the low-quality reads, trimming the adapters and contaminants formed by the adapters, and removing reads < 18 nt in length. Moreover, noncoding RNAs, including ribosomal RNA (rRNA), transfer RNA (tRNA), and small nuclear RNA (snRNA), were eliminated based on reference sequences from Rfam (http://rfam.janelia.org/) and piRNA (http://pirnabank.ibab.ac.in/). Afterward, the clean reads were mapped to known miRNA precursors, and the mature miRNAs were deposited in miRBase 19.0 (available online: http://www.mirbase.org/). Unmappable sequences were used to predict putative novel candidate miRNAs with the Mfold RNA folding prediction web server (available online: http://mfold.rna.albany.edu/). The sequencing data were submitted to the Gene Expression Omnibus (GEO) database (www.ncbi.nlm.nih.gov/geo/) under accession number GSE94551.

2.4. Data analysis

Our previous study fully analyzed the known differentially expressed miRNAs. Therefore, in this study, we mainly focused on putative novel miRNAs to further excavate new information capable of explaining the differences between EV71 and CA16 infections.

2.4.1. Principal component analysis (PCA)

After data preprocessing, PCA plots of the samples were created using the clean data for all the putative novel miRNAs through median centering of the data set to determine the similarities and discriminations among groups.

2.4.2. Differential analysis of putative novel miRNAs

The samples were normalized by calculating the tags per million total RNA reads (TPM) and used to compare the relative abundances of the specific miRNAs within each data set. After calculating the fold changes, putative novel miRNAs with a P value ≤.05 (chi-square test) and a fold change ≥2 or ≤ 0.5 were identified as differentially expressed miRNAs. All unique and shared differentially expressed miRNAs in these groups are presented in a Venn diagram.

2.4.3. Unsupervised hierarchical clustering

Unsupervised hierarchical clustering is often used to achieve clustering of different miRNAs and groups of samples and to enable detection of differential expression patterns of miRNAs among different groups. First, we defined the differentially expressed miRNAs using log2-fold changes in the ratios of the detected signals [log2 (infected vs. control)]. Then, unsupervised hierarchical clustering analyses of the differentially expressed miRNAs were performed using the R computer program. Correlation similarity matrixes and complete linkage algorithms were used for the cluster analyses.

2.4.4. Trend analysis

To identify pivotal differences between the EV71- and CA16-infected samples, we conducted trend analyses of the differentially expressed putative novel miRNAs by paying close attention to putative novel miRNAs with opposite expression trends. The secondary structures of these miRNAs were predicted by Mfold RNA.

2.4.5. Target prediction of putative novel miRNAs

The potential targets of these putative novel miRNAs with opposite expression patterns were predicted by two miRNA target prediction algorithms (miRanda and RNAhybrid) (Lewis et al., 2003; Rehmsmeier et al., 2004). The parameters for miRanda were a Score ≥150 and Energy < −20, and the parameter for RNAhybrid was Energy < −25. To increase the reliability of the results, only target genes identified by both databases were considered predicted target genes for these

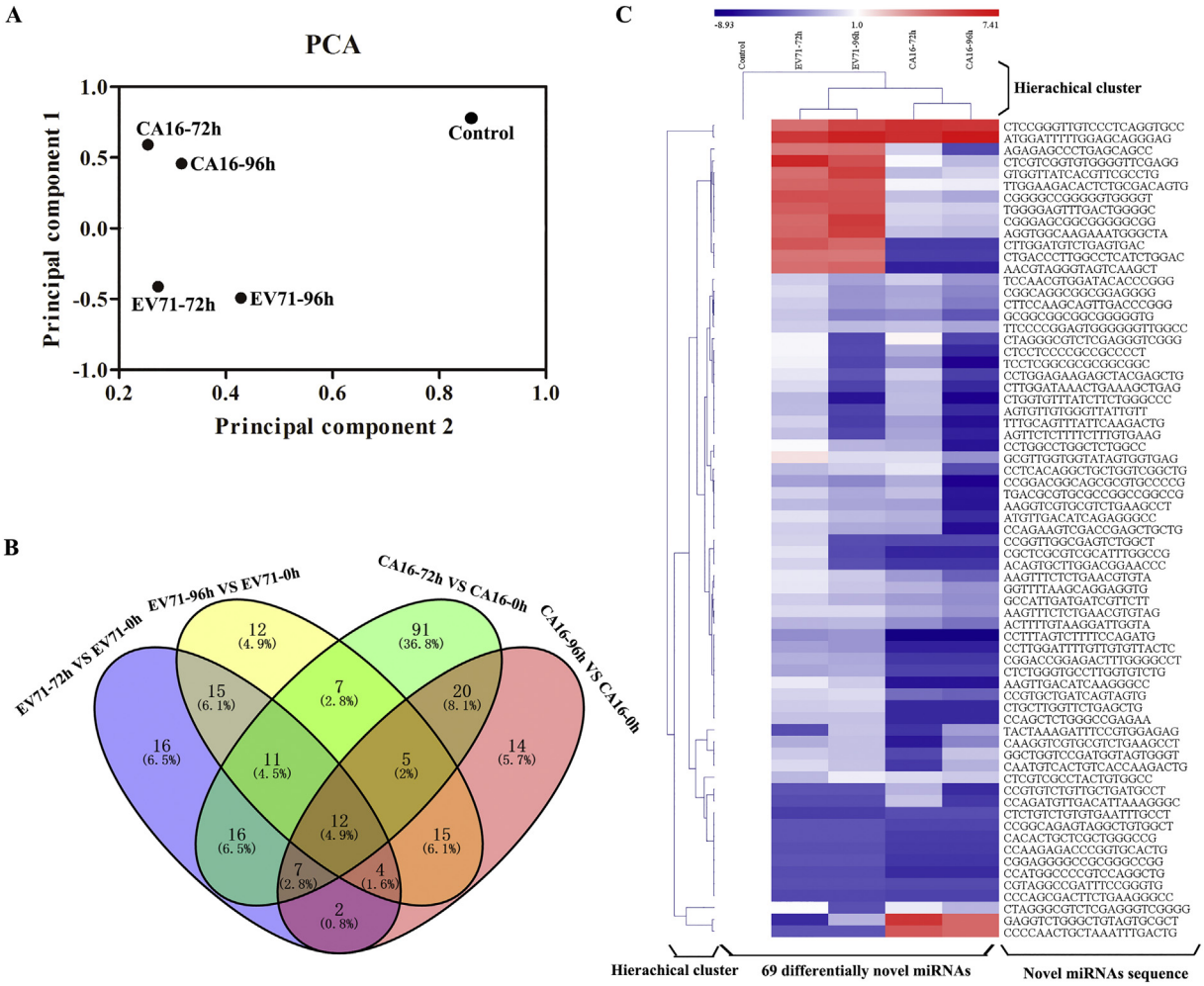

Fig. 1. (A) Principal component analysis (PCA) plot of the putative novel miRNA expression data from the infected samples and control subjects using the first two components. (B) Venn diagram of the individual group comparisons among the four sample groups. Each of the circles depicts the number of different miRNAs identified as statistically significant in the study. (C) Heat map diagram showing two-way hierarchical clustering of the putative novel miRNAs and samples. The clustering was performed using the complete-linkage method together with the Euclidean distance. Each row represents the sequence of a putative novel miRNA, and each column indicates a sample. The putative novel miRNA clustering tree is shown on the left. The colour scale illustrates the relative level of putative novel miRNA expression: red, below the reference channel; blue, higher than the reference. (For interpretation of the references to colour in this figure legend, the reader is referred to the web version of this article.)

miRNAs.

2.4.6. Gene ontology (GO) and Kyoto Encyclopedia of Genes and Genomes (KEGG) pathway analyses

The targets of the differentially expressed miRNAs were subjected to GO and KEGG pathway analyses using the DAVID online software (da Huang et al., 2009). Significantly enriched GO and pathway categories were determined based on the false discovery rate (FDR ≤ 0.05). The FDR was calculated based on the Fisher test method.

2.4.7. Regulatory network analysis

We constructed miRNA-regulatory networks between the miRNAs and targets, miRNAs and GO terms, and miRNAs and pathways to further reveal the fundamental functions of the miRNAs.

2.5. miRNA and miRNA target quantification by quantitative RT-PCR (qRT-PCR) in the validation set

qRT-PCR was used to validate the miRNAs identified using deep sequencing and to analyze their expression patterns. Moreover, to indirectly corroborate the miRNA expression results, the target mRNA levels were measured by qRT-PCR. Total RNA from three replicates per sample was isolated using the TRIzol (Tiangen, China) extraction method and subsequently cleaned up using RNeasy Mini Columns (Qiagen, Germany). For miRNA testing, equal quantities of RNA were polyadenylated and reverse transcribed into complementary DNA (cDNA) using the Mir-X miRNA First-Strand Synthesis Kit (Clontech, USA) according to the manufacturer's instructions. The cDNA of each sample was amplified with the SYBR Advantage qPCR Premix (Clontech, USA) on the 7500 Fast Real-time PCR system (Applied Biosystems, USA). The reactions were performed in a 96-well optical plate as follows: 95 °C for 10 s, 40 cycles of 95 °C for 10 s and 60 °C for 40 s, and dissociation at 95 °C for 60 s, 55 °C for 30 s and 95 °C for 30 s. For mRNA testing, qRT-PCR was also performed on the 7500 Fast Real-time PCR system using the One Step SYBR® PrimeScript™ RT-PCR Kit (TAKARA, Japan) in accordance with the manufacturer's recommendations. The amplification cycles were carried out under the following conditions: 1 cycle at 42 °C for 5 min and 1 cycle at 95 °C for 10 s, followed by a two-step procedure consisting of 5 s at 95 °C and 34 s at 60 °C for 40 cycles (with data collection at the end of the 60 °C step at each cycle) and dissociation at 95 °C for 60 s, 55 °C for 30 s and 95 °C for 30 s. The relative changes in the miRNA and mRNA expression levels were determined using the $2^{-\triangle\triangle Ct}$ method, with normalization to endogenous references (U6 snRNA and GAPDH, respectively). The

sequences of the primers used in this study are listed in Tables S1 and S2. All experiments were implemented in three biological and technical replicates.

2.6. Statistical analysis

For the sequencing data, raw reads obtained from each library were normalized to the TPM. For the qRT-PCR, the data are expressed as the mean ± standard error of the mean (SEM). The statistical analysis was conducted using SPSS 18.0 (IBM SPSS, USA). A *P*-value below 0.05 was considered statistically significant.

3. Results

3.1. Overview of putative novel miRNA sequencing data from HUVECs infected with EV71 and CA16

In our previous study, we evaluated the effects of EV71 and CA16 infections on the expression of known miRNAs in HUVECs using high-throughput small RNA sequencing (Song et al., 2017). Therefore, we aimed to analyze the expression levels and roles of putative novel miRNAs in this study. The putative novel miRNA expression data were normalized with the robust multichip average algorithm and converted to log2 values, which were used for PCA, hierarchical clustering and trend analyses. PCA was performed to identify the important axis of variability among the samples. The results showed clear separation between the control and infected groups (Fig. 1A). Moreover, the EV71- and CA16-infected samples grouped closely together (Fig. 1A). This result indicated notable disparity between the EV71-infected and CA16-infected groups.

3.2. Investigation into putative novel differentially expressed miRNAs and hierarchical clustering analysis

We obtained standard miRNA expression profiles after preprocessing the sequencing results and identified the putative novel differentially expressed miRNAs (FDR < 0.05 and log2FC ≥ 1), which are presented as a Venn diagram (Fig. 1B). The numbers of upregulated and downregulated putative novel differentially expressed miRNAs in the different groups are also shown in detail in Table S3. The heat map of putative novel differentially expressed miRNAs is displayed in Fig. 1C to further illustrate the differential expression patterns of the miRNAs between the EV71- and CA16-infected samples. A total of 69 putative novel miRNAs that were differentially expressed in at least one sample were utilized in the cluster analysis. The heat map diagram showed clear clustering of the infected samples and more dispersed clustering between the control and infected samples, which corroborated the PCA results. These results illustrated that the putative novel miRNA expression patterns induced by EV71 and CA16 might be both strain- and time-specific.

3.3. Trend analysis of the putative novel differentially expressed miRNAs

To evaluate the key miRNAs associated with the different outcomes between EV71 and CA16 infections, a trend analysis was performed to identify miRNAs with opposite expression patterns over time following EV71 and CA16 infection. As shown in Fig. 2A, 11 differentially expressed putative novel miRNAs were identified according to the abovementioned search method. Furthermore, these miRNAs were all upregulated by EV71 infection and no significant changes or a little downregulation by CA16 infection, suggesting that they might contribute significantly to the distinctions induced by the two viruses. The fold changes and reads of the 11 putative novel miRNAs are presented in Tables S4 and S5. Finally, secondary structure predictions demonstrated that the 11 putative novel miRNAs could fold into the hairpin structures typical of pre-miRNAs (Fig. 2B).

3.4. Functional enrichment analysis of the targets of the predicted miRNAs

To determine the regulatory functions of the 11 miRNAs with opposite expression trends, GO function and pathway enrichment analyses were performed for the predicted target genes. First, in the present study, targets of these putative novel miRNAs were identified based on sequence complementarities and the free energy of the predicted RNA duplex using miRanda and RNAhybrid. In total, 3485 target genes were obtained by miRanda, and 3359 target genes were obtained by RNAhybrid; a total of 2653 nonredundant target genes overlapped between the two data sets. Analysis of the GO processes and KEGG pathways in which the 2653 intersectional target genes were involved was performed using the DAVID tool, with thresholds of ≥ 2 gene counts and *P*-values $\leq .05$. The GO enrichment results illustrated the functions of these target mRNAs in three different categories: biological process (BP), molecular function (MF), and cell component (CC). The top 15 items significantly enriched by the target mRNAs for each of the three GO categories are shown in Fig. 3. The pathways further reveal the mechanisms of the miRNAs, and the top 15 significantly enriched terms are plotted in Fig. 4. Among these terms, the nervous system-related GO terms and pathways accounted for a large proportion (e.g., axonogenesis, axon guidance, synaptic transmission, neuronal cell body, neuron projection, and synapse). Thus, the GO and KEGG analyses provide a better understanding of the functions of the target genes and a reference for future research.

3.5. Integrated miRNA-target, miRNA-GO and miRNA pathway regulatory networks

To examine functional regulation from the miRNAs to their targets, we selected 175 overlapped genes derived from the GO and KEGG pathway analyses (Fig. 5A) and applied them to construct miRNA regulatory networks (Fig. 5B). In addition, based on the GO annotations and KEGG pathway analyses of these target genes, a miRNA-GO network (Fig. 5C) and a miRNA pathway network (Fig. 5D) were established, respectively. By analyzing the 3 regulatory networks, we demonstrated that the miRNAs exerted their complex functions by regulating their target genes with their associated GO terms and pathways in the HUVECs during the EV71 and CA16 infection processes.

3.6. qRT-PCR analysis confirmed putative novel differential expression of selected miRNAs and their targets in HUVECs

To confirm the deep sequencing results, we used qRT-PCR to assess the expression of 11 miRNAs. The relative level of each miRNA is shown in Fig. 6, which presents a trend similar to that of the miRNA high-throughput sequencing data. That is to say, these miRNAs were all upregulated by EV71 infection, but there were no significant changes or a little downregulation about these miRNAs in CA16 infection. Subsequently, we randomly chose 10 of the 175 targets to further measure and confirm the miRNA sequencing data. The expression levels of the target genes were relative inversely associated with the expression patterns of the miRNAs regulating these target genes (Fig. S1). The target gene corresponding to miRNA1 is CSDC2; the target genes corresponding to miRNA3 are NXPH4, CLDN15 and MAPK4; the target genes corresponding to miRNA4 are ENG, SDK2, NTNG2, TAL1, and NEUROD2; the target gene corresponding to miRNA10 is MNX1.

4. Discussion

HFMD, which is predominantly caused by EV71 and CA16, has emerged as a serious public health threat worldwide, particularly across the Asia-Pacific region (Li et al., 2017). However, the diverse molecular mechanisms of EV71- and CA16-host interactions remain poorly understood. Recently, miRNA profiling has become a topic of considerable interest in viral disease research, as researchers are searching for

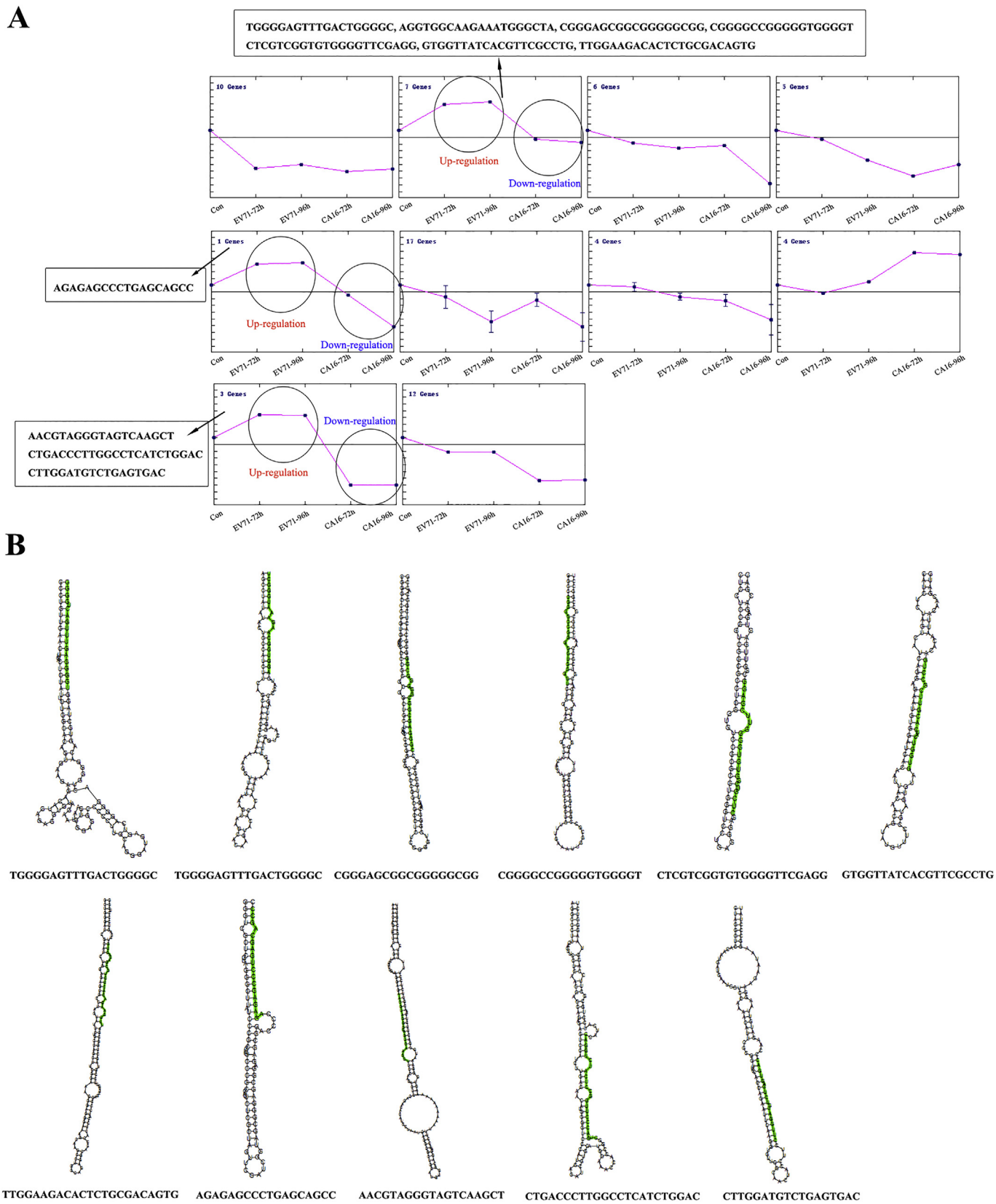

Fig. 2. (A) Trend analysis of the putative novel differentially expressed miRNAs in HUVECs in response to EV71 and CA16 infections at different time points post-infection. The putative novel miRNAs that showed opposite expression patterns during progression of the EV71 and CA16 infections are listed in boxes. (B) The locations and putative folded structures of these oppositely expressed putative novel miRNA precursors in humans. The mature miRNA is highlighted (green) in the stem-loop structures obtained using Mfold. (For interpretation of the references to colour in this figure legend, the reader is referred to the web version of this article.)

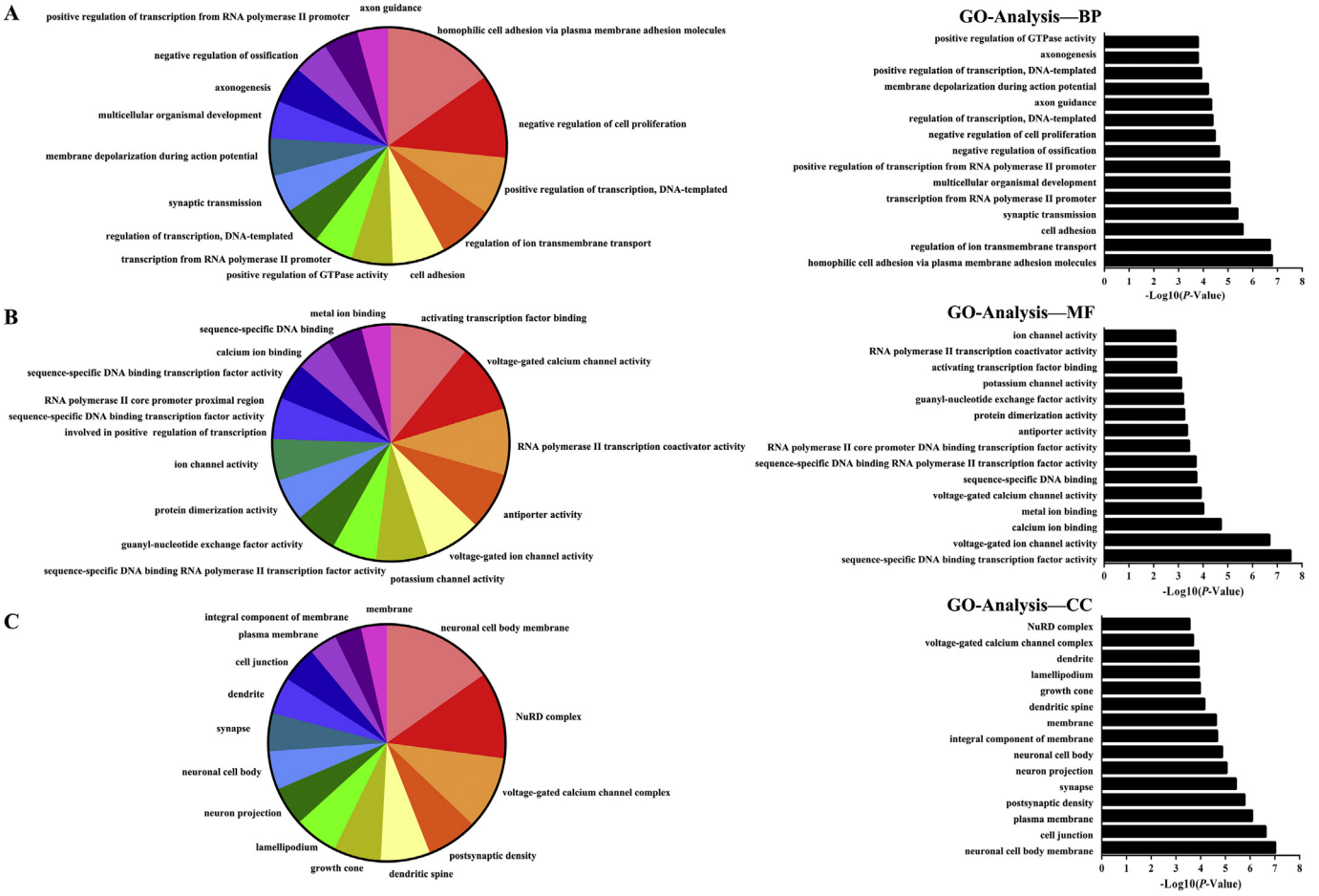

Fig. 3. Gene ontology enrichment terms for the putative miRNA targets. Pie charts of the top 15 enriched biological processes (A), molecular functions (B) and cellular components (C) are shown in the left panel. Bars indicate the *P* values of the GO terms annotated as unique GO terms and are presented in the right panel. The vertical axis is the GO category, and the horizontal axis is the negative logarithm of the *P* value.

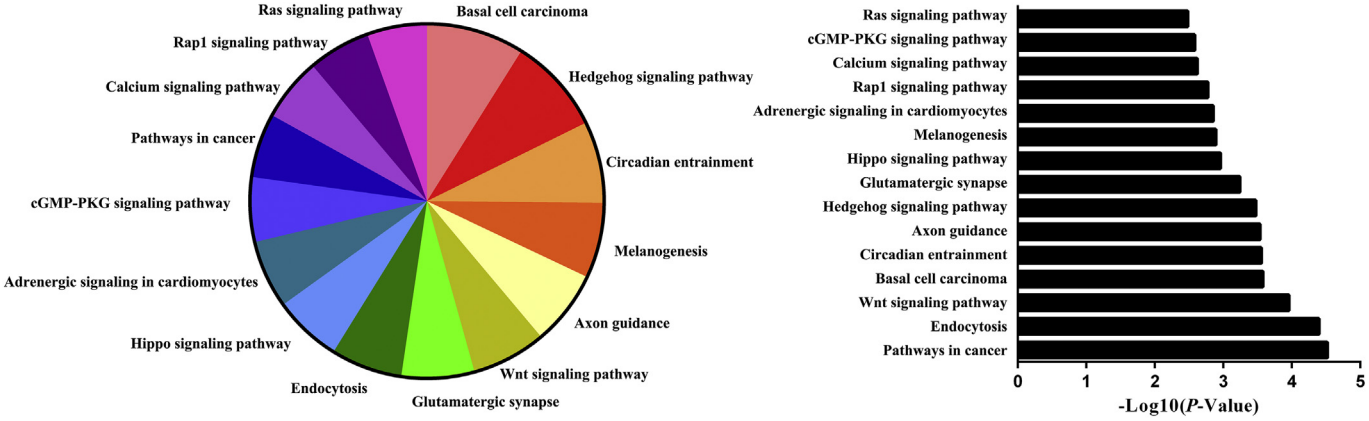

Fig. 4. The top 15 enriched pathways were analyzed with the predicted target genes of 11 putative novel miRNAs using the DAVID online software. Pathway enrichment annotations are provided in the pie charts in the left panel. The horizontal axis plots the negative log of the adjusted *P* value, and the vertical axis exhibits the pathway category in the bars of the right panel.

cellular targets that can be exploited to combat infection (Ho et al., 2016). For example, 79 and 203 differentially expressed miRNAs were identified in PBMCs from asymptomatic hepatitis B antigen carriers and chronic hepatitis B patients, respectively, compared to expression in healthy controls; after bioinformatics analysis, these miRNAs were considered biomarkers or potential therapeutic targets (Hou et al., 2017). Gao et al. first described the expression profiles of viral and cellular miRNAs in infectious mononucleosis caused by primary Epstein-Barr virus infection and noted that hsa-miR-155-5p in B cells and hsa-miR-18b-5p in $CD8^+$ T cells exhibited a positive correlation with EVB-miRNAs (i.e., miR-BHRF1–2-5p and miR-BART2-5p) (Gao et al., 2015). Additionally, many studies have explored the effects of miRNAs on EV71 and CA16 infections. For instance, miR-16-5p can mediate a positive feedback loop in EV71-induced apoptosis and suppress viral replication (Zheng et al., 2017). Cellular miRNAs, such as miR432*, can regulate replication of the CA16 virus in

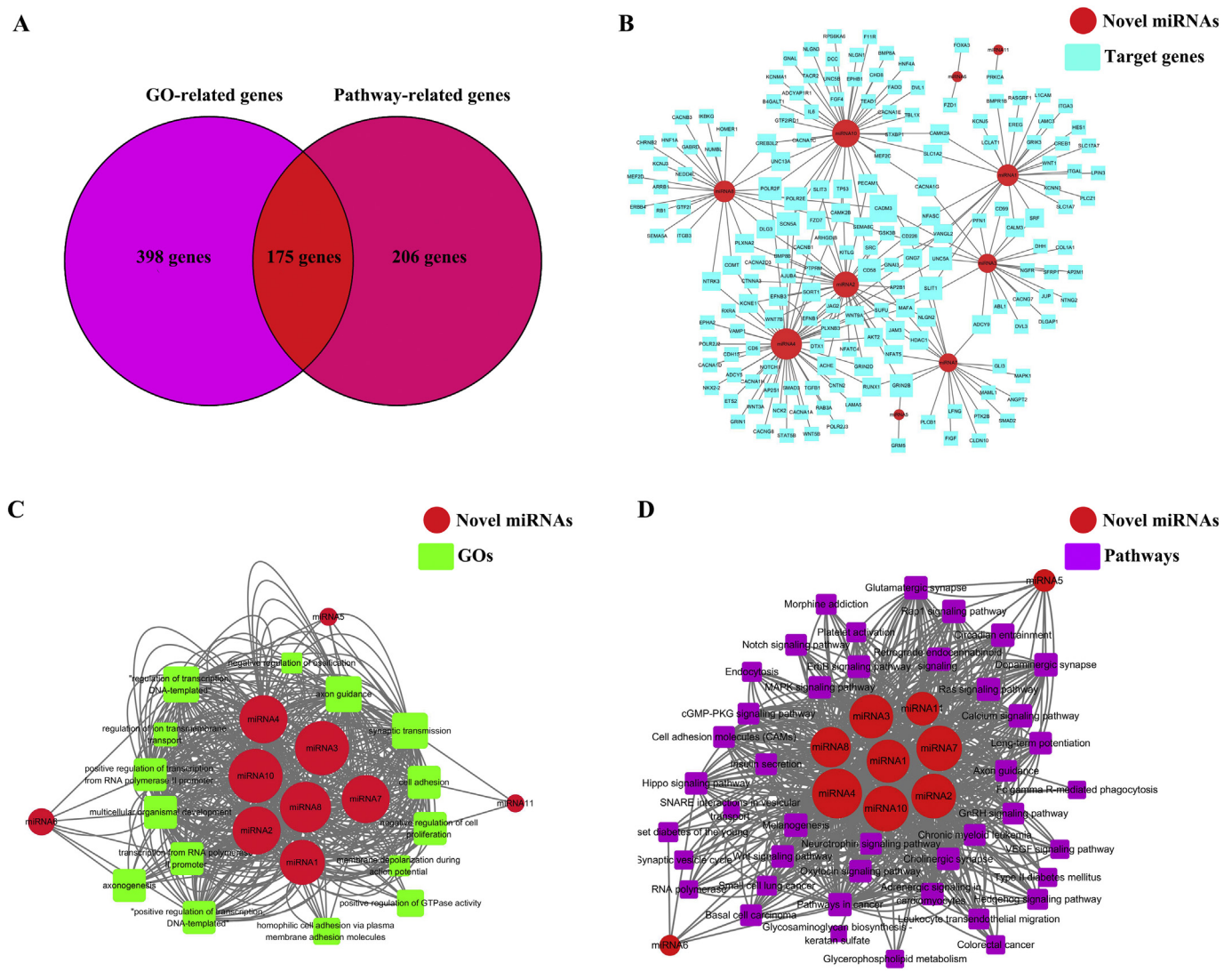

Fig. 5. Regulatory miRNA-target, miRNA-GO and miRNA-pathway networks after infection with EV71 and CA16. All red circles indicate putative novel miRNAs. The names of all miRNAs, targets, GO terms, and pathways are shown in the figure. The size of the nodes is relative to the importance of the miRNAs and other nodes. (A) The intersection of the GO-related and pathway-related genes. (B) miRNA-target network. The targets are displayed as rounded blue rectangles. (C) miRNA-GO network. GO term nodes are depicted as rounded green rectangles. Edges in the network represent the inhibitory effect of the miRNAs on the GO terms. (D) miRNA-pathway network. Purple rectangle-shaped nodes denote pathways. Edges indicate a negative correlation between the miRNAs and pathways. (For interpretation of the references to colour in this figure legend, the reader is referred to the web version of this article.)

rhabdomyosarcoma cells (Yang and Tien, 2014). Furthermore, our previous studies revealed that aberrant expression of known miRNAs played a critical role in the development and progression of EV71 and CA16 infections (Song et al., 2017). Therefore, in this report, we utilized next-generation sequencing (NGS) technology to analyze putative novel miRNA expression profiles in HUVECs infected with EV71 and CA16. We detected a total of 247 putative novel miRNAs with 2-fold differences in their expression levels between the infected and control groups. Moreover, of these miRNAs, only 69 putative novel differentially expressed miRNAs were expressed in all groups. The unsupervised hierarchical clustering analysis performed with a log2 fold change of these putative novel miRNAs showed clustering of the different miRNAs and sample groups, which enabled the detection of differential effects of the miRNAs in the different groups and suggested strain- and time-specific patterns in the HUVECs in response to EV71 and CA16 infections. More specific differentially expressed miRNAs were found in the CA16–72 h VS 0 h comparison than in the counterparts of the other groups. We speculated that one possible reason for this phenomenon might be that CA16 entered the HUVECs and initiated proliferation earlier than EV71. The titer at 12 h was higher in the CA16-infected group than in the EV71-infected group (Song et al., 2018); thus, more viral reproduction at an earlier stage may have led to the induction of more differentially expressed miRNAs in the CA16–72 h VS 0 h comparison than in the counterparts of the other groups.

To develop a better understanding of the roles of the deregulated putative novel miRNAs in association with the different outcomes induced by EV71 and CA16, we focused on miRNAs with opposite expression trends between the EV71- and CA16-infected cells. We found 11 putative novel miRNAs that displayed an inverse expression trend between the two virus infections. Furthermore, these miRNAs all gradually decreased and increased during the EV71 and CA16 infection time series, respectively. This result indicated that the different pathogenesis outcomes might result from regulation of putative novel miRNAs by EV71 and CA16. Subsequently, GO and pathway analyses of the potential targets of the 11 putative novel differentially expressed miRNAs were carried out to illuminate the underlying pathogenic mechanisms of EV71 and CA16. The GO terms and pathway annotations showed that nervous system-related GOs (i.e., axonogenesis, axon

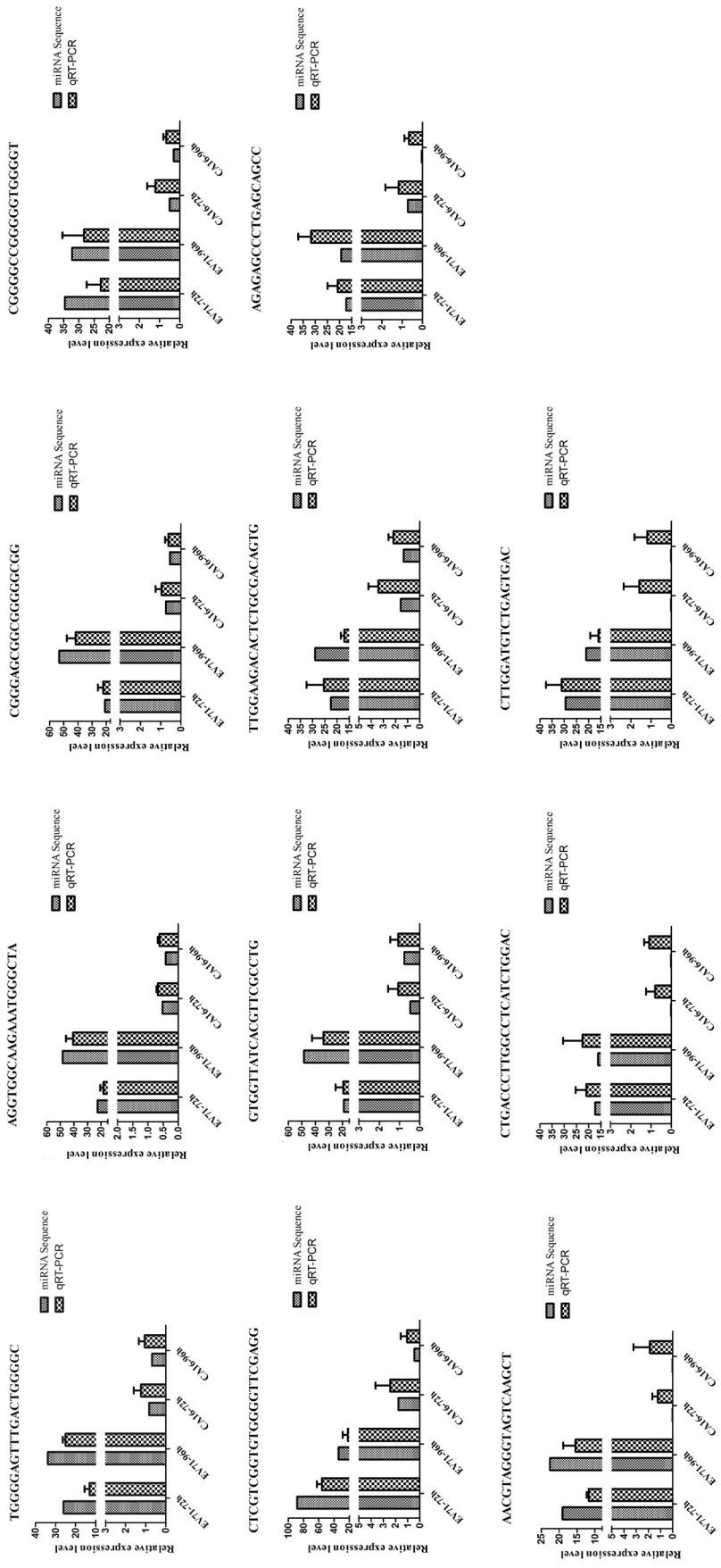

Fig. 6. The qRT-PCR validation of the putative novel miRNAs.

guidance, synaptic transmission, neuronal cell body, neuron projection, and glutamatergic synapse), adhesion-related GOs (i.e., hemophilic cell adhesion via plasma membrane adhesion molecules, cell adhesion, and cell junction), and cell proliferation-related GOs (i.e., negative regulation of cell proliferation, RNA polymerase II transcription coactivator activity, Wnt signaling pathway, and Ras signaling pathway) were significantly enriched. Feng et al. have reported that the preferential infection of astrocytes by EV71 plays a key role in the viral neurogenic pathogenesis , and astrocytes may contribute to viral encephalitis through their important neurobiological functions in the selective regulation of neural cell activities and the modulation of synaptic transmissions (Feng et al., 2016); thereby this result suggested that the GO term “synaptic transmission” might be related to CNS damage caused by HFMD. In addition, Ye et al. have demonstrated that the miR-126 played as a pivotal link the ERK1/2 and WNT/β-catenin signaling pathways and promoted CBV3 propagation (Ye et al., 2013). Moreover, Lu et al. have showed that calcium signaling pathway contributed to EV71-induced apoptosis (Lu et al., 2013). Thus these findings indicated that the Wnt signaling pathway and calcium signaling pathway in Pathway analysis might be associated with the replication and pathogenesis of enteroviruses. However, evidence of remarkable differences, especially in nervous system manifestations, between EV71 and CA16 infections is accumulating. EV71 and CA16 are both highly neurotropic viruses that can lead to the development of severe neurological symptoms. In general, EV71 infection more often results in neurological symptoms than CA16 infection and sometimes even leads to death (Ong and Wong, 2015). Therefore, central nervous system (CNS) inflammation is thought to be the principal underlying cause of EV71 pathogenesis (Tsai et al., 2014). Based on our results, we speculated that the nervous system-related GOs regulated by the putative novel differentially expressed miRNAs presented an increasing expression pattern during EV71 infection that might suppress the normal function of the nervous system based on the negative regulatory mechanisms of the miRNAs. In addition, the changes in the adhesion-related GO terms might reduce the adhesive forces among cells, which could impair cell-cell interactions in HUVECs infected with EV71. HUVECs are usually used to construct a cellular model of the blood-brain barrier (BBB) in vitro (Akiyama et al., 2000). Thus, destruction of HUVECs may elevate BBB permeability. Nevertheless, a growing number of reports has demonstrated two likely routes by which EV71 or CA16 invade the CNS: the viruses may be transmitted to the CNS from the blood across the BBB, or they may enter the CNS through retrograde axonal transport from the peripheral nerves (Denizot et al., 2012; Solomon et al., 2010). Hence, our results indicated that the novel inversely differentially expressed miRNAs generated in the HUVECs infected with EV71 and CA16 might initiate different degrees of HUVEC impairment, thus creating a relatively permissive environment for viral invasion into the brain and contributing to the different EV71 and CA16 infection outcomes in the CNS. Finally, the current study's establishment of regulatory networks provides new insights into the interactions between miRNAs and targets, miRNAs and GO terms, and miRNAs and signaling pathways, all of which contribute to viral pathogenesis. The miRNA expression profile in HEK 293 T cells after CA16 infection had been reported. SLC19A1, ITGA3, and PRRC2B appeared in both the target gene predictions for these miRNAs and in our predicted miRNA-targeted genes. Moreover, their pathway analysis showed that the circadian rhythm pathway was notably enriched, which was consistent with the results of our study, indicating that changes in miRNAs and their target genes caused by CA16 infection might have a certain commonality even in different types of infected cells. Finally, some differences in changes in miRNAs and their corresponding targets were noted (Jin et al., 2017).

In summary, using small RNA sequencing technology and bioinformatics approaches, this study demonstrated that EV71 and CA16 infections resulted in specific putative novel miRNA expression patterns in HUVECs. Although we have conducted a comprehensive analysis of known and novel differentially expressed miRNA profiles and functions, which group of miRNAs may play a key role in the infection process is unknown. The viral infection process is very complicated, and the screened known and novel differential miRNAs may be collectively implicated in regulation of the viral infection process instead of only a specific group of miRNAs. In our current studies, we focused on the analysis of miRNA profiles, but the more detailed mechanisms still need further exploration. Additionally, discrepant biological functions and pathways regulated by the oppositely expressed miRNAs during EV71 and CA16 infections may be key reasons for the different outcomes between EV71 and CA16 infections. Furthermore, construction of detailed regulatory networks revealed a global perspective for exploring miRNA-mediated mechanisms. Notably, the widespread utility of our findings is somewhat limited given that cell culture is not necessarily reflective of the molecular pathogenesis of the virus in an in vivo setting. Therefore, this study provides useful insights that may help elucidate the different host-pathogen interactions following EV71 and CA16 infections but requires further in vivo research.

Supplementary data to this article can be found online at https://doi.org/10.1016/j.meegid.2019.06.007.

Acknowledgments

This study is funded by the CAMS Innovation Fund for Medical Sciences (2016-I2M-1-014), National Natural Sciences Foundations of China (31700153 and 81373142), Fundamental Research Funds for the Central Universities and PUMC Youth Fund (2017310039), Yunnan Applied Basic Research Projects (2018FB026), Medical Reserve Talents of Yunnan Province Health and Family Planning (H-2017034) and Yunnan Major Science and Technology Projects (2018ZF006). The funders had no role in the study design, data collection and analysis, decision to publish, or preparation of the manuscript.

Ethical approval

This article does not contain any studies with human participants or animals performed by any of the authors.

Conflict of interest

The authors declare that they have no conflicts of interest.

References

Akiyama, H., Kondoh, T., Kokunai, T., Nagashima, T., Saito, N., Tamaki, N., 2000. Blood-brain barrier formation of grafted human umbilical vein endothelial cells in athymic mouse brain. Brain Res. 858, 172–176.

da Huang, W., Sherman, B.T., Lempicki, R.A., 2009. Systematic and integrative analysis of large gene lists using DAVID bioinformatics resources. Nat. Protoc. 4, 44–57.

Denizot, M., Neal, J.W., Gasque, P., 2012. Encephalitis due to emerging viruses: CNS innate immunity and potential therapeutic targets. J. Inf. Secur. 65, 1–16.

Feng, M., Guo, S., Fan, S., Zeng, X., Zhang, Y., Liao, Y., Wang, J., Zhao, T., Wang, L., Che, Y., Wang, J., Ma, N., Liu, L., Yue, L., Li, Q., 2016. The preferential infection of astrocytes by Enterovirus 71 plays a key role in the viral neurogenic pathogenesis. Front. Cell. Infect. Microbiol. 6, 192.

Gao, L., Ai, J., Xie, Z., Zhou, C., Liu, C., Zhang, H., Shen, K., 2015. Dynamic expression of viral and cellular microRNAs in infectious mononucleosis caused by primary Epstein-Barr virus infection in children. Virol. J. 12, 208.

He, S.Z., Chen, M.Y., Xu, X.R., Yan, Q., Niu, J.J., Wu, W.H., Su, X.S., Ge, S.X., Zhang, S.Y., Xia, N.S., 2017. Epidemics and aetiology of hand, foot and mouth disease in Xiamen, China, from 2008 to 2015. Epidemiol. Infect. 145, 1865–1874.

Ho, B.C., Yu, S.L., Chen, J.J., Chang, S.Y., Yan, B.S., Hong, Q.S., Singh, S., Kao, C.L., Chen, H.Y., Su, K.Y., Li, K.C., Cheng, C.L., Cheng, H.W., Lee, J.Y., Lee, C.N., Yang, P.C., 2011. Enterovirus-induced miR-141 contributes to shutoff of host protein translation by targeting the translation initiation factor eIF4E. Cell Host Microbe 9, 58–69.

Ho, B.C., Yang, P.C., Yu, S.L., 2016. MicroRNA and pathogenesis of enterovirus infection. Viruses 8.

Hou, X., Liang, Y., Chen, J., Wei, Y., Zeng, P., Wang, L., Lu, C., Diao, H., 2017. Expression profiling of cellular MicroRNA in asymptomatic HBsAg carriers and chronic hepatitis B patients. Biomed. Res. Int. 2017, 6484835.

Hu, Y., Song, J., Liu, L., Li, J., Tang, B., Wang, J., Zhang, X., Zhang, Y., Wang, L., Liao, Y., He, Z., Li, Q., 2016. Different microRNA alterations contribute to diverse outcomes

following EV71 and CA16 infections: insights from high-throughput sequencing in rhesus monkey peripheral blood mononuclear cells. Int. J. Biochem. Cell Biol. 81, 20–31.
Hu, Y., Song, J., Liu, L., Li, J., Tang, B., Zhang, Y., Wang, J., Wang, L., Fan, S., Feng, M., Li, Q., 2017. Comparison analysis of microRNAs in response to EV71 and CA16 infection in human bronchial epithelial cells by high-throughput sequencing to reveal differential infective mechanisms. Virus Res. 228, 90–101.
Jin, J., Li, R., Jiang, C., Zhang, R., Ge, X., Liang, F., Sheng, X., Dai, W., Chen, M., Wu, J., Xiao, J., Su, W., 2017. Transcriptome analysis reveals dynamic changes in coxsackievirus A16 infected HEK 293T cells. BMC Genomics 18, 933.
Lewis, B.P., Shih, I.H., Jones-Rhoades, M.W., Bartel, D.P., Burge, C.B., 2003. Prediction of mammalian microRNA targets. Cell 115, 787–798.
Li, J., Wang, J., Xu, C., Yin, Q., Hu, M., Sun, Z., Shao, D., 2017. Hand, foot, and mouth disease in mainland China before it was listed as category C disease in May, 2008. Lancet Infect. Dis. 17, 1017–1018.
Lu, J.R., Lu, W.W., Lai, J.Z., Tsai, F.L., Wu, S.H., Lin, C.W., Kung, S.H., 2013. Calcium flux and calpain-mediated activation of the apoptosis-inducing factor contribute to enterovirus 71-induced apoptosis. J. Gen. Virol. 94, 1477–1485.
Mao, Q., Wang, Y., Yao, X., Bian, L., Wu, X., Xu, M., Liang, Z., 2014. Coxsackievirus A16: epidemiology, diagnosis, and vaccine. Human Vaccin. Immunother. 10, 360–367.
Mao, Q.Y., Wang, Y., Bian, L., Xu, M., Liang, Z., 2016. EV71 vaccine, a new tool to control outbreaks of hand, foot and mouth disease (HFMD). Expert Rev. Vaccin. 15, 599–606.
Ong, K.C., Wong, K.T., 2015. Understanding enterovirus 71 neuropathogenesis and its impact on other neurotropic enteroviruses. Brain Pathol. 25, 614–624.
Pourianfar, H.R., Grollo, L., 2015. Development of antiviral agents toward enterovirus 71 infection. J. Microbiol. Immunol. Infect. 48, 1–8.
Reed, Z., Cardosa, M.J., 2016. Status of research and development of vaccines for enterovirus 71. Vaccine 34, 2967–2970.
Rehmsmeier, M., Steffen, P., Hochsmann, M., Giegerich, R., 2004. Fast and effective prediction of microRNA/target duplexes. RNA 10, 1507–1517.
Solomon, T., Lewthwaite, P., Perera, D., Cardosa, M.J., McMinn, P., Ooi, M.H., 2010. Virology, epidemiology, pathogenesis, and control of enterovirus 71. Lancet Infect. Dis. 10, 778–790.
Song, J., Hu, Y., Li, J., Zheng, H., Wang, J., Guo, L., Ning, R., Li, H., Yang, Z., Fan, H., Liu, L., 2017. Different microRNA profiles reveal the diverse outcomes induced by EV71 and CA16 infection in human umbilical vein endothelial cells using high-throughput sequencing. PLoS One 12, e0177657.
Song, J., Hu, Y., Li, H., Huang, X., Zheng, H., Hu, Y., Wang, J., Jiang, X., Li, J., Yang, Z., Fan, H., Guo, L., Shi, H., He, Z., Yang, F., Wang, X., Dong, S., Li, Q., Liu, L., 2018. miR-1303 regulates BBB permeability and promotes CNS lesions following CA16 infections by directly targeting MMP9. Emerg. Microb. Infect. 7, 155.
Tsai, J.D., Kuo, H.T., Chen, S.M., Lue, K.H., Sheu, J.N., 2014. Neurological images and the predictors for neurological sequelae of epidemic herpangina/hand-foot-mouth disease with encephalomyelitis. Neuropediatrics 45, 102–108.
Wang, J., Qi, S., Zhang, X., Zhang, Y., Liu, L., Che, Y., He, Z., Zhao, Y., Lu, S., Yu, W., Li, Q., 2014. Coxsackievirus A 16 infection does not interfere with the specific immune response induced by an enterovirus 71 inactivated vaccine in rhesus monkeys. Vaccine 32, 4436–4442.
Wen, B.P., Dai, H.J., Yang, Y.H., Zhuang, Y., Sheng, R., 2013. MicroRNA-23b inhibits enterovirus 71 replication through downregulation of EV71 VPl protein. Intervirology 56, 195–200.
Yang, Z., Tien, P., 2014. MiR432* regulate the replication of coxsackievirus A16 in rhabdomyosarcoma cells. Acta Microbiol. Sin. 54, 679–687.
Ye, X., Hemida, M.G., Qiu, Y., Hanson, P.J., Zhang, H.M., Yang, D., 2013. MiR-126 promotes coxsackievirus replication by mediating cross-talk of ERK1/2 and Wnt/beta-catenin signal pathways. Cell. Mol. Life Sci. 70, 4631–4644.
Zheng, Z., Ke, X., Wang, M., He, S., Li, Q., Zheng, C., Zhang, Z., Liu, Y., Wang, H., 2013. Human microRNA hsa-miR-296-5p suppresses enterovirus 71 replication by targeting the viral genome. J. Virol. 87, 5645–5656.
Zheng, C., Zheng, Z., Sun, J., Zhang, Y., Wei, C., Ke, X., Liu, Y., Deng, L., Wang, H., 2017. MiR-16-5p mediates a positive feedback loop in EV71-induced apoptosis and suppresses virus replication. Sci. Rep. 7, 16422.